

Dielectric capping effects on binary and ternary topological insulator surface states

Jiwon Chang,* Priyamvada Jadaun, Leonard F. Register, Sanjay K. Banerjee, and Bhagawan Sahu
Microelectronics Research Center, The University of Texas at Austin, Austin Texas 78758

(Dated: September 25, 2021)

Using a density functional based electronic structure method, we study the effect of crystalline dielectrics on the metallic surface states of Bismuth- and chalcogen-based binary and ternary three dimensional topological insulator (TI) thin films. Crystalline quartz (SiO_2) and boron nitride (BN) dielectrics were considered. Crystalline approximation to the amorphous quartz allows to study the effect of oxygen coverage or environmental effects on the surface states degradation which has gained attention recently in the experimental community. We considered both *symmetric* and *asymmetric* dielectric cappings to the surfaces of TI thin films. Our studies suggest that BN and quartz cappings have negligible effects on the Dirac cone surface states of both binary and ternary TIs, except in the case of an oxygen-terminated quartz surface. Dangling bond states of oxygens in oxygen-terminated quartz dominate the region close to Fermi level, thereby distorting the TI Dirac cone feature and burying the Dirac point in the quartz valence band region. Passivating the oxygen-terminated surface with atomic hydrogen removes these dangling bond states from the Fermi surface region, and consequently the clear Dirac cone is recovered. Our results are consistent with recent experimental studies of TI surface degradation in the presence of oxygen coverage.

PACS numbers: 71.15.Dx, 71.18.+y, 73.20.At, 73.61.Le

I. INTRODUCTION

Three dimensional (3D) topological band insulator (TI) Bi_2X_3 ($\text{X}=\text{Se}, \text{Te}$) and its ternary counterparts have attracted considerable attention from the condensed matter physics community because of the relatively simple crystal structure that hosts novel surface states^{1,2}, and their unusual responses to external fields. Many more 3D TI materials have been predicted³⁻⁷ by now, and quest for studying their novel surface state properties, in isolation as well as in presence of other materials, has increased in recent years. The 3D TI surface states are time-reversal symmetric (TRS) at high-symmetry points in the momentum space and are therefore protected against perturbations which cannot break TRS such as non-magnetic impurities or adatoms. Such novel properties have caused excitement in the electron device community as well because it can be a potential alternative to graphene as a channel material in field effect transistors. The advances in understanding of structural, electronic, magnetic and transport properties of 3D TI, made possible by both experimental and theoretical studies⁸⁻¹⁰, can provide important informations for novel applications. Beside the fundamental studies of these model 3D TI materials, theoretically, no studies of dielectric effects on the surface states have been performed so far from first principles. We address dielectric effects on the TI surface states using *ab-initio* density functional theory (DFT) and semi-local density approximation¹¹. Two crystalline dielectrics were considered: quartz (SiO_2) and boron nitride (BN). Both binary TI Bi_2Se_3 and ternary TIs $\text{Bi}_2\text{Se}_2\text{Te}$ and $\text{Bi}_2\text{Te}_2\text{Se}$ were considered for this study. Our studies suggest that neither of the two dielectrics has an effect on the Dirac cone except the oxygen-terminated quartz. Under the environment of oxygen dangling bond, the Dirac cone on the

TI surface is buried inside the quartz valence band continuum with the oxygen dangling bond states occupying the region around the Fermi level. Surface passivation by atomic hydrogen pushes the dangling bond states from the Fermi surface region down below Fermi level and a clear Dirac cone emerges at the Fermi level. These findings are consistent with recent experimental studies of surface degradation effects in the presence of oxygen¹⁴.

We begin by describing the thin film structures of both binary and ternary TIs, built from their bulk hexagonal structures, and the computational method in section II. In section III, we present the dielectric capping effects, by BN and SiO_2 , on their metallic surface states. Both *symmetric* and *asymmetric* cappings are explored. Finally we present our summary and conclusions.

II. ISOLATED THIN FILMS AND COMPUTATIONAL APPROACH

The thin film structures for both binary and ternary TIs are constructed by stacking up several quintuple layers (or QLs: 1QL=5 atomic layers) along the crystallographic z -direction with a vacuum region of 3 nm which forms the supercell in the DFT calculation. The first principle calculations were performed using the OPENMX code¹⁵, based on a linear combination of pseudoatomic orbital (PAO) method¹⁶. The pseudopotentials were generated from full relativistic calculations, and the generalized gradient approximation¹¹ was applied for the exchange-correlation potential. The kinetic energy cut-off of 180 Rydberg and the \mathbf{k} -point mesh of $7 \times 7 \times 1$ for Brillouin zone (BZ) integration (Fig. 1(c)) were used. The basis sets were carefully chosen to reproduce previous bulk and thin film calculations. The cut-off, \mathbf{k} -point mesh and vacuum region were optimized to guarantee the convergence of the results and their agreement with

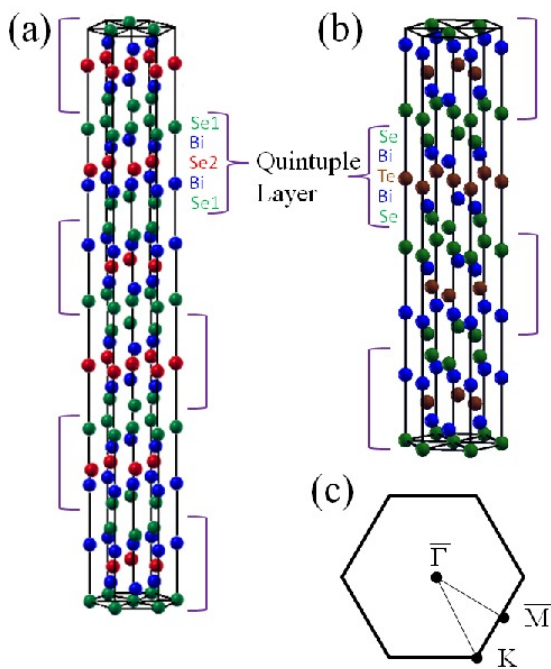


FIG. 1: (Color online) Schematic diagram of (a) 6QLs Bi_2Se_3 and (b) 4QLs $\text{Bi}_2\text{Se}_2\text{Te}$ thin film structures obtained by stacking QLs along the z -direction. (c) Two-dimensional Brillouin zone (BZ) of the (111) surface of thin film TIs with three time-reversal invariant points $\bar{\Gamma}$, \bar{M} , and \bar{K} .

previous theoretical calculations.

For the binary TI, previous theoretical studies of bulk Bi_2Se_3 found the computed lattice parameters close to the experimental values⁸, so we used the experimental lattice parameters $a=0.41388$ nm and $c=2.8633$ nm in the hexagonal unit cell and optimized bulk atomic positions to build the thin film structure. For the ternary TI $\text{Bi}_2\text{Se}_2\text{Te}$ ($\text{Bi}_2\text{Te}_2\text{Se}$), we built thin film structures with the bulk hexagonal unit cell lattice parameters $a=0.422$ nm (0.428 nm) and $c=2.92$ nm (2.99 nm) in the previous theoretical calculation¹⁹, and optimized the thin film structure by letting atoms move along z -direction. We optimized thin film structures only for ternary TIs, since atomic relaxations significantly affect the band structure of thin film $\text{Bi}_2\text{Se}_2\text{Te}$ around the Dirac point¹⁹. We considered the thin film of 6QLs and 4QLs for binary and ternary TIs, respectively, since previous studies on binary^{17,18} and ternary¹⁹ TIs suggest that 6QLs and 4QLs are the minimum thicknesses to maintain the gapless surface state at the Dirac point. We also obtained the same critical thickness values by our own calculations. In the calculated band structure of 6QLs Bi_2Se_3 , we could observe the Dirac cone within a bulk gap of 0.262 eV. For the ternary TIs $\text{Bi}_2\text{Se}_2\text{Te}$ and $\text{Bi}_2\text{Te}_2\text{Se}$, Dirac cone surface states reside inside the bulk gap of 0.204 eV and 0.325 eV, respectively.

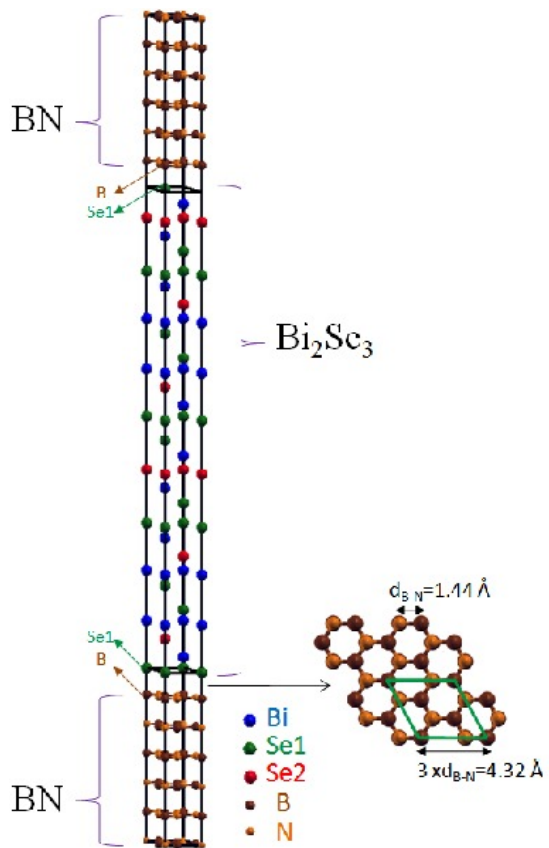


FIG. 2: (Color online) Schematic diagram of the supercell structure of BN and 6QLs Bi_2Se_3 . The colors corresponding to the atoms are labeled on the bottom right of supercell. The green and brown arrows at the top and bottom interfaces indicate B on the top of Se. The top view of bottom interfacial atomic layers is shown on the bottom right of the supercell structure. The 1×1 Bi_2Se_3 cell (green rhombus) is matched with $3d_{B-N} \times 3d_{B-N}$ BN. This corresponds to *symmetric* capping mentioned in the text. Also Se on the top of N on both sides of the film corresponds to *symmetric* case.

III. THIN FILMS WITH SYMMETRIC AND ASYMMETRIC DIELECTRIC CAPPINGS

We chose crystalline SiO_2 in order to assess the effect of oxygen environment on the TI surface states. The choice of BN dielectrics is perhaps guided by the recent graphene transport experiments using crystalline dielectrics^{12,13}. We considered both *symmetric* and *asymmetric* cappings in terms of relative orientations of TI and dielectric surface atoms. *Asymmetry* in terms of different dielectrics on two opposite TI surfaces was not considered.

The bulk structures of both dielectrics were studied with the computational parameters described in the previous section. For the hexagonal BN, the experimental lattice parameters are: $a=0.2494$ nm and $c=0.666$ nm with the distance between B and N $d_{B-N}=0.144$ nm²⁰, and the band gap is 5.97 eV²¹. We used the experimental val-

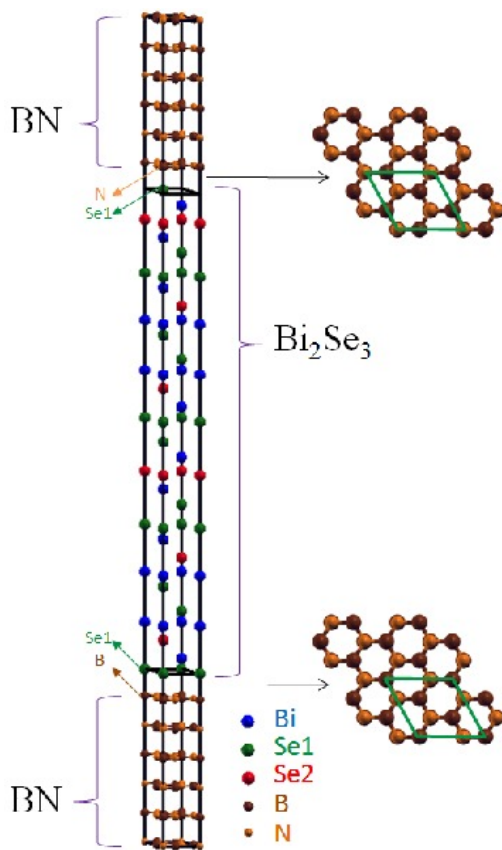


FIG. 3: (Color online) Same as Fig. 2 but now the B on the top of Se on one side and N on the top of Se on the other side of the TI thin film. The colors corresponding to atoms are labeled on the bottom right of supercell. The green, brown, and orange arrows indicate the relative position of Se atom with respect to B (bottom) and N (top). The top views of top and bottom interfacial atomic layers are shown on the top right and bottom right of the supercell, respectively. The 1×1 Bi_2Se_3 cell (green rhombus) is matched with $3d_{B-N} \times 3d_{B-N}$ BN. This corresponds to *asymmetric* capping in the text.

ues of lattice constants and atomic positions. With these experimental values, our calculated bulk band gap value is 5.5 eV close to the experimental value 5.97 eV. The hexagonal crystal structure of quartz contains fourfold coordinated oxygens, forming a layered structure with Si with the experimental lattice parameters ($a=0.4914$ nm and $c=0.5408$ nm²²). Our DFT calculations of optimized lattice parameters with semi-local potentials are found to be close to these experimental values, accurate to within 0.1%. Therefore, we chose experimental lattice parameters for building our interface structures of TI and quartz. The bulk quartz SiO_2 has a direct band gap of 9 eV²³, and our DFT calculation of crystalline SiO_2 results in a band gap value of 9.4 eV. We note that our results obtained for quartz should be considered at best qualitative with regard to TIs capped with amorphous SiO_2 .

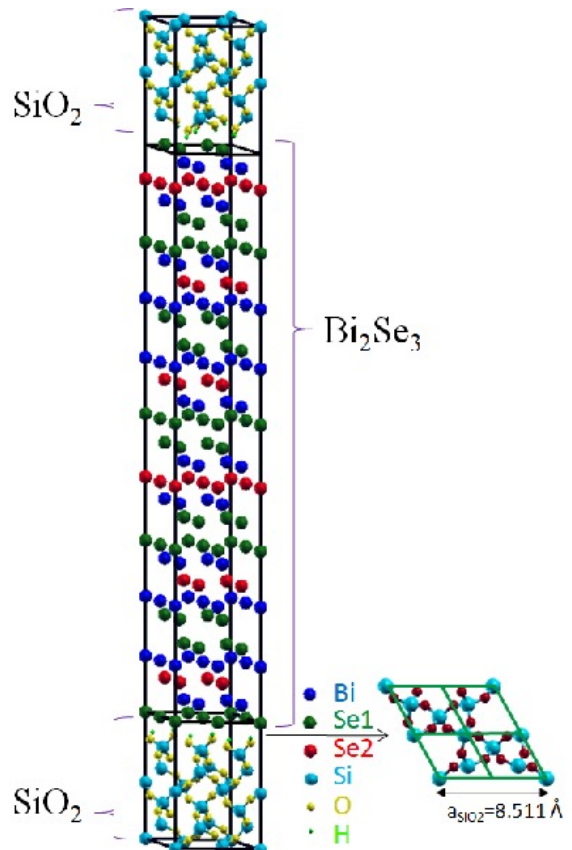


FIG. 4: (Color online) Schematic diagram of oxygen-terminated quartz with dangling bond states covered with hydrogen atoms (small green circles) interfaced on both sides of Bi_2Se_3 . Si-terminated surface also possesses dangling bonds, but only oxygen-terminated surface without the hydrogen coverage distorts the surface state Dirac cone. The top view of bottom interfacial atomic layers is shown on the bottom right of the supercell structure. The 2×2 Bi_2Se_3 cell (green rhombus) is matched with 1×1 SiO_2 at the interface.

A. Thin Films of Binary TI Bi_2Se_3 with Dielectrics

In this section, we discuss the thin film of binary TI Bi_2Se_3 .

1. Construction of Supercell Structure

The interface structures are built by putting the dielectric material on the surfaces of 6QLs of Bi_2Se_3 film stacked along the z -direction (since it has no band gap for the surface states). In constructing supercells, we maintained the TI lattice and strained the dielectrics to fit with the TI surface resulting in the compressive or tensile strain on the dielectrics to focus on their effects on the TI electronic structure. For the BN, our analysis suggests that to keep our computational burden in DFT-based calculations minimal, $3d_{B-N} \times 3d_{B-N}$ lattice structure can be matched in-plane with 1×1 Bi_2Se_3 cell

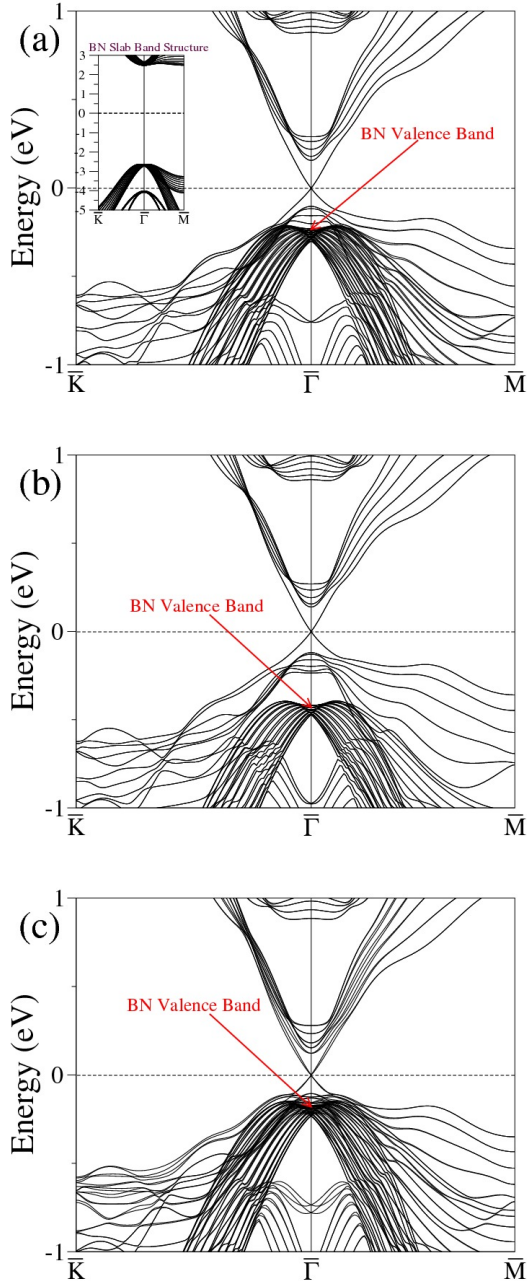


FIG. 5: Band structures of $\text{Bi}_2\text{Se}_3/\text{BN}$ supercell along high symmetry directions of the hexagonal BZ for *symmetric* capping case (a) B on the top of Se and (b) N on the top of Se on both sides of TI film without atomic relaxation. The Dirac cone and its degeneracy at the $\bar{\Gamma}$ -point are not disturbed in the presence of crystalline BN thin film. (c) Same case of (a) with atomic relaxation. Atomic relaxation has little effect on the Dirac cone feature. The position of BN valence band maximum can be found by the band structure of BN slab without TI in the inset of (a) and the DOS plots in Fig. 6.

(Fig.2 and Fig.3) or any multiples of this combination which maintains 3:1 matching ratio resulting in the 4.19% compressive strain on BN (in Table I). Other combina-

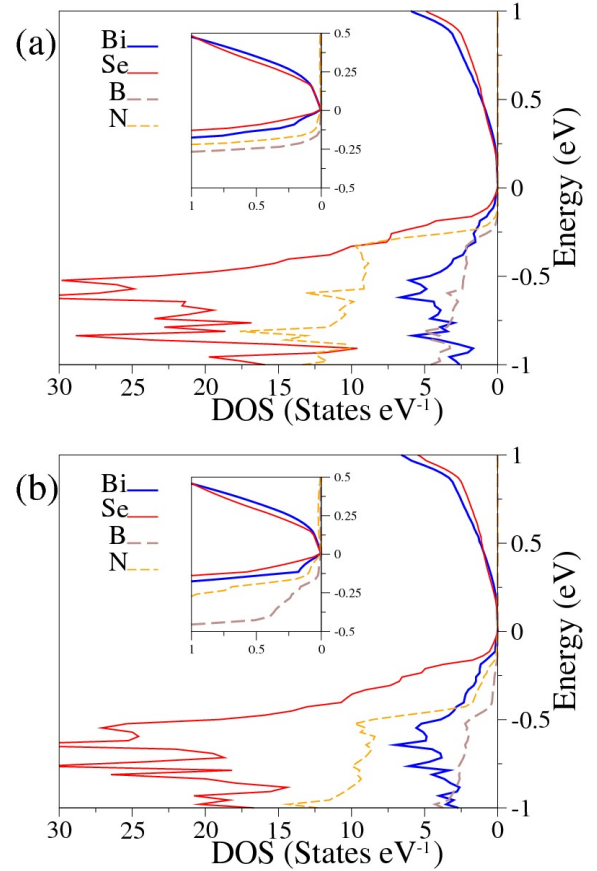


FIG. 6: (Color online) The atom-projected DOS in the same energy range as the band structures in Fig. 5 for *symmetric* capping cases (a) B on the top of Se and (b) N on the top of Se on both sides of TI film without atomic relaxation. Se orbitals are not in *resonance* with either B or N orbitals near the Fermi level suggesting that the Dirac cone, formed from the Bi and Se orbitals, is intact.

tions to allow less strain result in either difficulty in forming the periodic structure or larger supercells with orders of magnitude more atoms. Along the stacking direction, 6QLs of Bi_2Se_3 ($\sim 6\text{nm}$) is put on six atomic layers of BN ($\sim 1.7\text{nm}$). The choice of 6 BN layers is somewhat arbitrary and guided by the fact that the size of vacuum and BN layers should be thick enough to avoid interactions of periodically repeated Bi_2Se_3 surface layers. We also relaxed the interfacial atoms to assess its effects. For the SiO_2 dielectric, the supercell structure consists of two unit cells of SiO_2 sandwiching 6QLs Bi_2Se_3 . The size of SiO_2 and Bi_2Se_3 cell along x - y direction chosen is, respectively, 1×1 and 2×2 (Fig. 4) to minimize the computational cost. This produces about 2.75% compressive strain on both sides of SiO_2 as in Table I. Consideration of larger sizes can lead to the lower strain, but the total number of atoms in the cell increases at least an order of magnitude (250 versus 2500).

We considered four configurations of Se positions on the TI surfaces with respect to boron and nitrogen po-

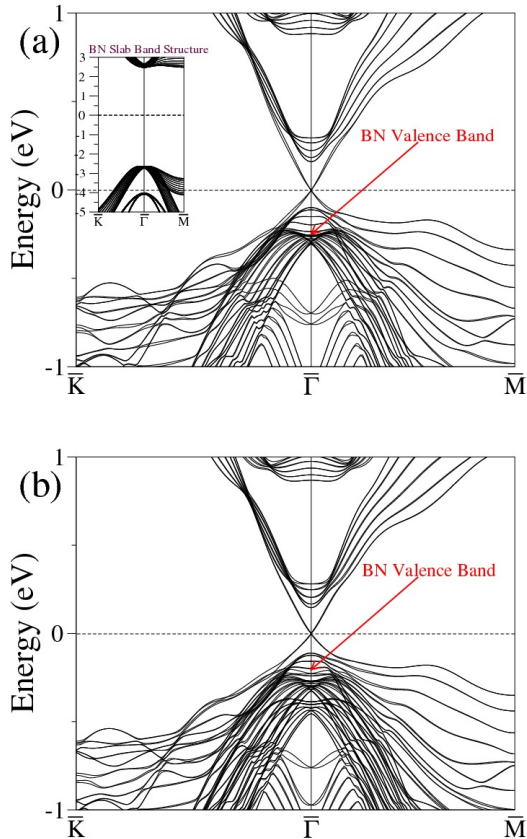


FIG. 7: Band structures of $\text{Bi}_2\text{Se}_3/\text{BN}$ supercell along high symmetry directions of the hexagonal BZ for *asymmetric* capping cases (a) B on the top of Se on one side and vacuum on the other side of TI film and (b) B on the top of Se atom on one side and N on the top of Se atom on the other side without atomic relaxation. The Dirac cone and its degeneracy at the $\bar{\Gamma}$ -point are not disturbed in the presence of crystalline BN thin film. The position of BN valence band maximum can be found by the band structure of BN slab without TI in the inset of (a) and the DOS plots in Fig. 8.

sitions on the BN layer: Se on the top of B, on the top of N, on the hexagonal hole and on the bond between B and N atoms. Two surface terminations, Si and oxygen, of quartz were considered. Our calculations suggests that all BN configurations are energetically close and provide quite similar band structures. Therefore, we had a choice in the selection of a particular configuration for further studies. We chose the case of B or N on the top of Se on both TI surfaces. We refer the structure of B or N on the top of Se on both sides of TI film as *symmetric* capping (Fig. 2). The structures of B on the top of Se on one side and N on the top of Se on the other side of TI film, or only B or N on one side of TI film and vacuum on the other side, are referred as *asymmetric* capping (Fig. 3). For quartz, both TI surfaces capped with either oxygen-terminated or Si-terminated quartz were considered. Because quartz is a fourfold coordinated structure,

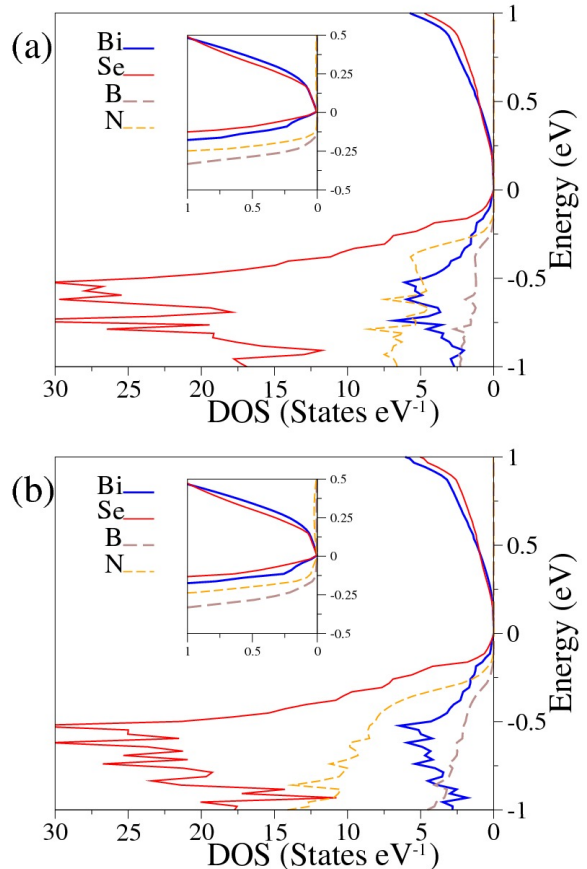


FIG. 8: (Color online) The atom-projected DOS in the same energy range as the band structures in Fig. 7 for *asymmetric* capping cases (a) B on the top of Se on one side and vacuum on the other side of TI film and (b) B on the top of Se on one side and N on the top of Se on the other side of TI film without relaxation. Se orbitals are not in *resonance* with either B or N orbitals near the Fermi level suggesting that Dirac cone, formed from the Bi and Se orbitals, is intact.

both of the surface terminations of quartz possess dangling bonds. Therefore, for quartz we also considered the dangling bond saturation with hydrogen, that is, hydrogen passivation of the quartz surfaces.

To set the optimal distance between the BN and Bi_2Se_3 layers at the interface, we performed the total energy calculations at the chosen set of interfacial distances. Our studies suggest an optimal distance of 0.3 nm for the case of the Se layer in Bi_2Se_3 on the top of either B or N in BN. For Bi_2Se_3 on quartz, the interfacial distances for Si and oxygen quartz terminations with and without hydrogen passivation need to be considered. Our studies suggest an optimal distance of 0.3 nm for Si-terminated surface, regardless of whether dangling bonds are saturated or not. For the oxygen-terminated quartz with hydrogen passivation, we found the optimal distance to be 0.25 nm. We considered these optimal interfacial distances in our further studies.

We considered the atomic relaxation in the interfacial

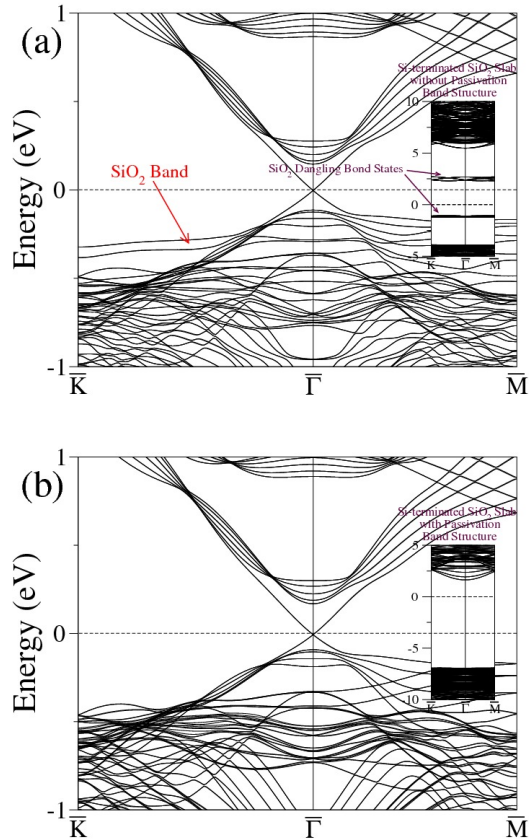


FIG. 9: Band structure of Bi_2Se_3 with Si-terminated quartz supercell along high symmetry directions in the hexagonal BZ (a) without hydrogen coverage and (b) with hydrogen coverage. The Dirac cone of TI is preserved in both cases. Insets of (a) and (b) show the band structures of only Si-terminated SiO_2 slab without and with passivation, respectively. In the inset of (b), a clear band gap is seen, while additional bands by Si dangling bond lie inside the gap in the inset of (a).

region in order to check its effect on the electronic structure of TI surface states. Two cases were considered: first is the case of Se on the top of B atom on both sides of TI with the initial optimal separation of 0.3 nm. We let atoms close to the interface (Bi/Se atoms in the top and bottom QLs and B/N atoms in the two layers next to TI surfaces) move in the z -direction. The second choice is that the oxygen-terminated quartz with the saturation of dangling bonds is put on both TI surfaces with optimal separation of 0.25 nm. Bi/Se atoms in the top and bottom QLs as well as Si/O atoms next to the TI surfaces are allowed to move in the z -direction, while hydrogen atoms used to saturate dangling bonds are relaxed in all directions.

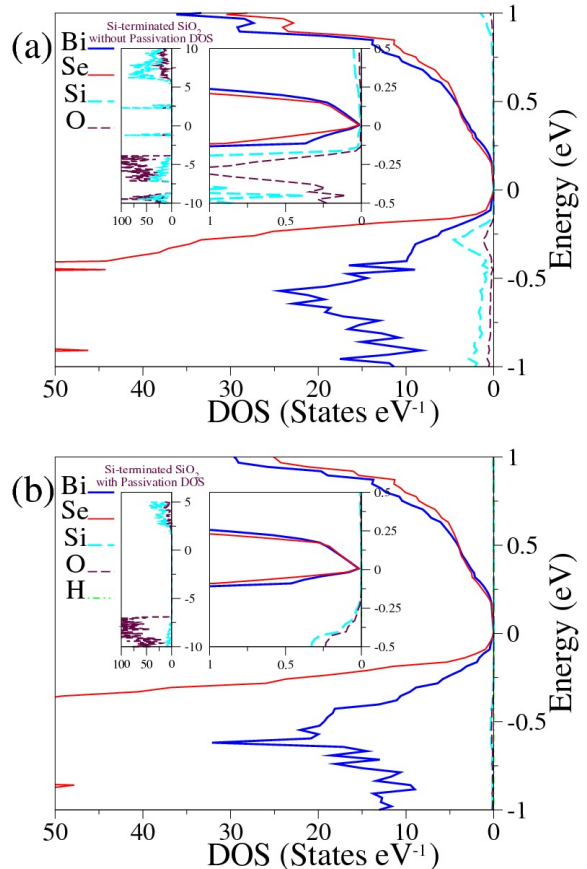


FIG. 10: (Color online) The atom-projected DOS in the same energy range as the band structures in Fig. 9 for the Si-terminated quartz cases (a) without hydrogen passivation and (b) with hydrogen passivation. The orbitals of Si and Se do not overlap near the Fermi level. Left insets of (a) and (b) show the atom-projected DOS for only Si-terminated SiO_2 slab without and with passivation, respectively. States from Si orbitals are clearly shown in the left inset of (a).

2. Results and Discussion

We first discuss the BN interface effects followed by the effects due to quartz surface terminations. Figs. 5(a) and (b), respectively, show the band structures of 6QLs Bi_2Se_3 capped on both sides by BN with either B on the top of Se atom or N on the top of Se atom (*symmetric* capping). The atomic relaxation is not considered here. The Dirac cone and its degeneracy are protected in both cases. This insensitivity of the Dirac cone to the presence of dielectric hints at negligible interactions be-

TABLE I: Hexagonal unit cell lattice constant a of binary TI and strains on dielectrics by the lattice mismatch at the interface

TI	a (nm)	Strain on SiO_2	Strain on BN
Bi_2Se_3	0.41388	2.75% compressive	4.19% compressive

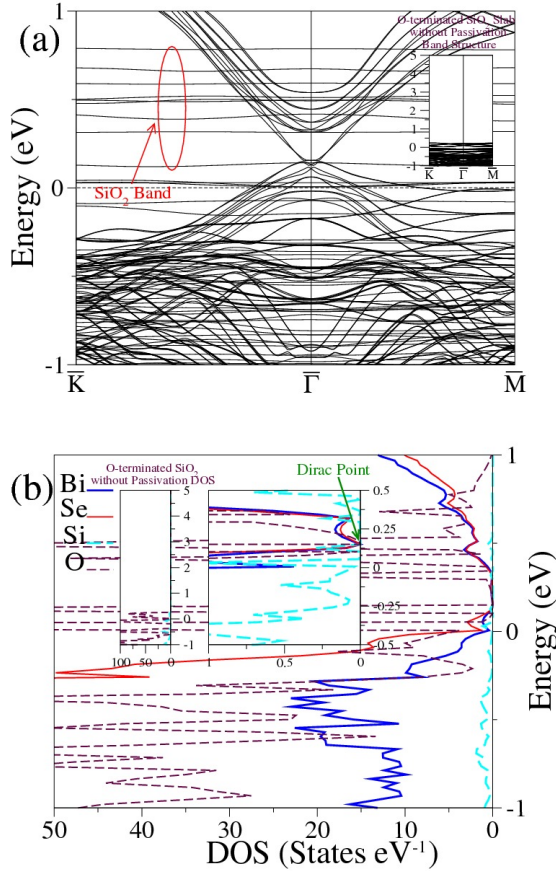


FIG. 11: (Color online) (a) Band structure of Bi_2Se_3 with oxygen-terminated quartz supercell without atomic relaxation along high symmetry directions in the hexagonal BZ suggesting that Dirac cone is significantly affected and (b) corresponding atom-projected DOS. The strong hybridization of Se and oxygen orbitals near the Fermi level is observed. Band structure of only oxygen-terminated SiO_2 slab without passivation is in the inset of (a), and corresponding the atom-projected DOS plot is shown in the left inset of (b). The Fermi level is below valence band edge formed by oxygen orbitals. The Dirac point is marked with the arrow on the right inset of (b).

tween B or N orbitals with Se orbitals. We confirm this hypothesis by plotting atom-projected DOS in the same energy range as the band structures in Figs. 6(a) and 6(b). These plots show that both B and N orbitals are not in *resonance* with the Se orbitals of TI. As a result, the Dirac cone surface states are protected. From the band structure of only BN atomic layers without Bi_2Se_3 (inset in Fig. 5(a)) and the atom-projected DOS plots of Figs. 6(a) and 6(b), the BN valence band maximum is estimated to be about 0.25 eV and 0.45 eV below the Dirac point for B on the top of Se atom and N on the top of Se atom cases, respectively. The band structure including the effect of atomic relaxation for the structure of B on the top of Se on both sides is shown in Fig. 5(c). Comparison Fig. 5(c) with Fig. 5(a) indicates

that the relaxation of interfacial atomic positions does not affect the essential characteristics of surface states near the Fermi surface. Fourfold degeneracy at the Dirac point and the dispersion relation still remain same, while valence bands of BN are a bit shifted close to the Dirac point. The bulk band gap size for each case (0.259 eV for B on the top of Se, 0.258 eV for N on the top of Se) does not change much from that of only 6QLs Bi_2Se_3 (0.262 eV).

In case of *asymmetric* capping, B on the top of Se atom on one side and vacuum on the other side of the TI film shows that the Dirac point degeneracy is still unaffected in Fig. 7(a). However, there is some splitting of valence and conduction bands close to it. With B on the top of Se on one side and N on the top of Se on the other side, the Dirac cone is not influenced either as seen in Fig. 7(b). Again, the atom-projected DOS plots in Figs. 8(a) and 8(b) suggest that this insensitivity is due to non-overlap of B and N orbitals with the Se orbitals. The position of BN valence band maximum is about 0.25 eV below the Fermi level for both cases similarly in the *symmetric* capping both TI surfaces with B on the Se, since B is placed on Se on one side of TI in both *asymmetric* cappings. The bulk band gap sizes are 0.268 eV and 0.257 eV for 'B on the top of Se atom on one side and vacuum on the other side' and 'B on the top of Se on one side and N on the top of Se on the other side', respectively.

For Si-terminated SiO_2 , both without and with dangling bond passivations show the protected Dirac cone surface state (Figs. 9(a) and 9(b)), consistent with the DOS plots in Figs. 10(a) and 10(b). Si orbitals do not mix with Se orbitals in the energy range close to the Dirac point. The band structure of only Si-terminated quartz slab without the passivation (inset of Fig. 9(a)) and its DOS plot (left inset of Fig. 10(a)) show the Si dangling bond states within the bulk quartz band gap. These dangling bond states are also observed around the energy level of -0.26 eV in the band structure of Si-terminated quartz with Bi_2Se_3 (Fig. 9(a)), which is confirmed by the peak value of DOS from Si orbitals at -0.26 eV in Fig. 10(a). By the hydrogen passivation, dangling bond states are removed in the band gap of only Si-terminated SiO_2 Slab as seen in the inset of Fig. 9(b) and the left inset of Fig. 10(b). As a result, we cannot find the SiO_2 states in the energy range of $-1 \sim 1$ eV in Figs. 9(b) and 10(b).

Fig. 11(a) is the band structure of the TI surface in the presence of oxygen-terminated quartz without passivation. The DOS plot (Fig. 11(b)) shows that oxygen orbitals lie close to the Se orbitals and dominate the region around Fermi level. By the effect of oxygen orbitals, the Dirac cone feature is significantly distorted. However, the Dirac point still remains intact, which can be confirmed by the linear increase of Bi and Se DOS around 0.15 eV in the right inset of Fig. 11(b). It exists close to the Fermi level and is buried inside SiO_2 valence band continuum as shown in Figs. 11(a) and 11(b). In the band

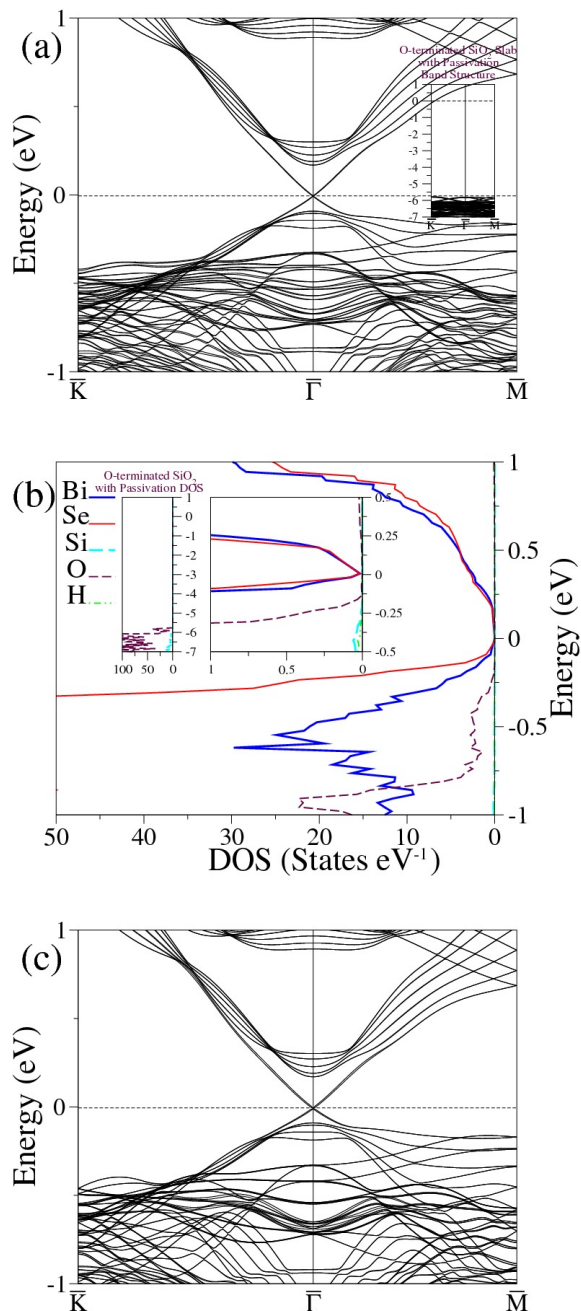


FIG. 12: (Color online) Same as Fig. 11 but now with hydrogen coverage of oxygen dangling orbitals (a) band structure without atomic relaxation and (b) corresponding atom-projected DOS. The Dirac cone of TI is recovered due to non interaction of Se and oxygen orbitals. (c) Same case with atomic relaxation. The Dirac cone feature is not affected by the atomic relaxation. Band structure of only oxygen-terminated SiO_2 slab with passivation is in the inset of (a), and corresponding the atomic-projected DOS plot is shown in the left inset of (b). The Fermi level is inside the gap.

structure of only oxygen-terminated quartz without hydrogen passivation, the Fermi level is under the valence

band edge in the inset of Fig. 11(a). When oxygen-terminated quartz is put on the surface of Bi_2Se_3 , the Fermi levels of two materials align, thereby pushing the Dirac point under the quartz valence band. Recent experimental studies of environmental effects on TI surface suggest the charge doping due to presence of oxygen¹⁴, but argue on the insensitiveness of TI Dirac cone. With oxygen surface passivation with atomic hydrogen, we recover a clear Dirac cone with the degeneracy point at the Fermi level (Fig. 12(a)) which is consistent with the DOS plots in Fig. 12(b). In the only oxygen-terminated quartz slab with passivation, we can observe that the Fermi level resides inside the band gap from the band structure and DOS plot shown in the inset of Fig. 12(a) and the left inset of Fig. 12(b), respectively. Therefore, the Fermi level matching between quartz and Bi_2Se_3 occurs without pulling down the Dirac cone surface states into the quartz valence band. Atomic relaxations of interfacial atoms has no effect on the Dirac cone as well as its degeneracy (Fig. 12(c)). For all SiO_2 cappings, except oxygen-terminated quartz without passivation, the Dirac cones reside inside the bulk band gap of about 0.26 eV.

B. Thin Films of Ternary TIs $\text{Bi}_2\text{Se}_2\text{Te}$ and $\text{Bi}_2\text{Te}_2\text{Se}$

In this section, we address the dielectric effects on the electronic structure of ternary TIs of Bi and Chalcogen.

1. Construction of Supercell Structure

The construction of interface structures for ternary TI $\text{Bi}_2\text{Se}_2\text{Te}$ ($\text{Bi}_2\text{Te}_2\text{Se}$) is similar with that for Bi_2Se_3 except the thickness of TI films. Since 4QLs is predicted as a minimum thickness to preserve the Dirac cone band structure for ternary TIs¹⁹, 4QLs thick TI films are used in the ternary TI calculations instead of 6QLs in the interface structure of binary TI Bi_2Se_3 with dielectrics.

For the BN dielectric capping, the BN of $3d_{B-N} \times 3d_{B-N}$ lattice structure is matched in-plane with the 1×1 $\text{Bi}_2\text{Se}_2\text{Te}$ ($\text{Bi}_2\text{Te}_2\text{Se}$) cell. Since we keep the lattice constant of $\text{Bi}_2\text{Se}_2\text{Te}$ ($\text{Bi}_2\text{Te}_2\text{Se}$) and fit BN into it, BN is under about 0.23% compressive strain (0.92% compressive strain) in Table II. Six layers of BN ($\sim 1.7\text{nm}$) is put on each side of 4QLs $\text{Bi}_2\text{Se}_2\text{Te}$ ($\text{Bi}_2\text{Te}_2\text{Se}$). For the SiO_2 dielectric, the 1×1 SiO_2 cell

TABLE II: Hexagonal unit cell lattice constant a of ternary TIs and strains on dielectrics by the lattice mismatch at the interface

TI	a (nm)	Strain on SiO_2	Strain on BN
$\text{Bi}_2\text{Se}_2\text{Te}$	0.422	0.83% compressive	0.23% compressive
$\text{Bi}_2\text{Te}_2\text{Se}$	0.428	0.57% tensile	0.92% compressive

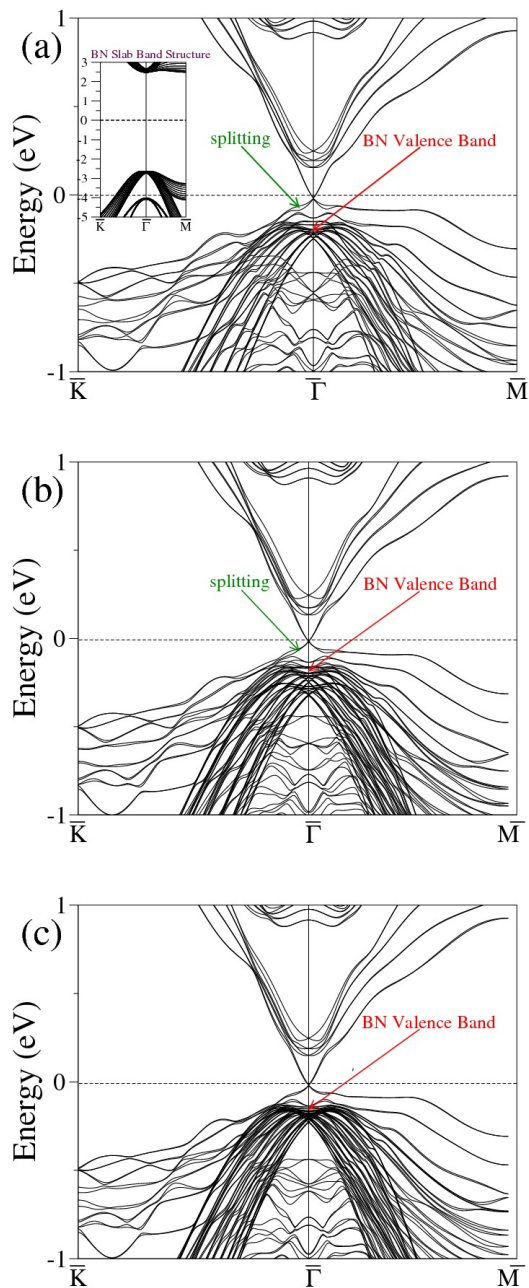


FIG. 13: Band structure of $\text{Bi}_2\text{Se}_2\text{Te}/\text{BN}$ supercell along high symmetry directions of the hexagonal BZ for *asymmetric* capping cases (a) B on the top of Se on one side and vacuum on the other side of TI film and (b) B on the top of Se atom on one side and N on the top of Se atom on the other side and for *symmetric* capping case (c) B on the top of Se on both sides of TI film. The atomic relaxation is not considered. The Dirac cone and its degeneracy at the $\bar{\Gamma}$ -point are not disturbed in the presence of crystalline BN thin film. The position of BN valence band edge can be estimated by the band structure of BN slab without TI in the inset of (a).

is fit with the 2×2 $\text{Bi}_2\text{Se}_2\text{Te}$ ($\text{Bi}_2\text{Te}_2\text{Se}$) cell in-plane, which results in 0.83% compressive strain (0.57% tensile

strain) on SiO_2 as summarized in Table II. Two unit cells of SiO_2 is stacked on both sides of 4QLs $\text{Bi}_2\text{Se}_2\text{Te}$ ($\text{Bi}_2\text{Te}_2\text{Se}$) in the z -direction.

Four configurations of Se (Te) positions on the TI surfaces with respect to B and N positions on the BN layer were investigated and found to be energetically quite similar, same as our studies on the binary TI with BN. The optimal distance between BN and $\text{Bi}_2\text{Se}_2\text{Te}$ ($\text{Bi}_2\text{Te}_2\text{Se}$), minimizing the total energy, is found to be 0.32 nm (0.3 nm). We considered *asymmetric* capping, B on the top of Se (Te) on one side and vacuum on the other side or B on the top of Se (Te) on one side and N on the top of Se (Te) on the other side, as well as *symmetric* capping, B on the top of Se (Te) on both sides. For the SiO_2 capping, we focused on the oxygen-terminated SiO_2 on both sides of TI without saturating oxygen dangling bond states as a critical case because there are reports, as discussed in the previous section, that oxygen dangling bond states may play a crucial role in modifying TI surface. Only $\text{Bi}_2\text{Te}_2\text{Se}$ with oxygen-terminated quartz was studied because we know that Se orbitals lie close in energy with the oxygen orbitals from the previous study of Bi_2Se_3 and the ternary TI $\text{Bi}_2\text{Se}_2\text{Te}$ is structurally similar to the binary TI Bi_2Se_3 regarding the atom species Se of top and bottom surfaces. Atomic relaxation was not considered for ternary TIs because the rearrangement of atomic positions was found to have no substantial effect in the binary TI with dielectrics.

2. Results and Discussion

Computed band structures of $\text{Bi}_2\text{Se}_2\text{Te}/\text{BN}$ supercell are seen in Fig. 13. Both *asymmetric* capping, in Fig. 13(a) (B on the top of Se on one side and vacuum on the other side) and Fig. 13(b) (B on the top of Se on one side and N on the top of Se on the other side), and *symmetric* capping in Fig. 13(c) (B on the top of Se on both sides) indicate that the Dirac point and the surface state dispersion are preserved. However, small splitting between top and bottom surface bands occurs in the *asymmetric* case, which are induced by different environments on opposite surfaces, while no such splitting exists in the *symmetric* structure. The valence band maximum is about 0.25 eV below for all three cases as we can estimate from the band structure of only BN slab in the inset of Fig. 13(a) and atom-projected DOS plots (figures not shown). The bulk band gap sizes (around 0.251 eV) in all BN cappings for $\text{Bi}_2\text{Se}_2\text{Te}$ increases a little bit as compared with the bulk gap (0.204 eV) of only 4QLs $\text{Bi}_2\text{Se}_2\text{Te}$.

Fig. 14 shows band structures of $\text{Bi}_2\text{Te}_2\text{Se}/\text{BN}$ supercell. In Fig. 14(a), the *asymmetric* capping of B on the top of Te on one side and vacuum on the other side, the fourfold degeneracy at the Dirac point is maintained, but two opposite surface bands seem to split. Another *asymmetric* capping that Te is on the top of B on one side and N on the other side leads to the split of fourfold degeneracy into two twofold degeneracies at the $\bar{\Gamma}$ -point. The

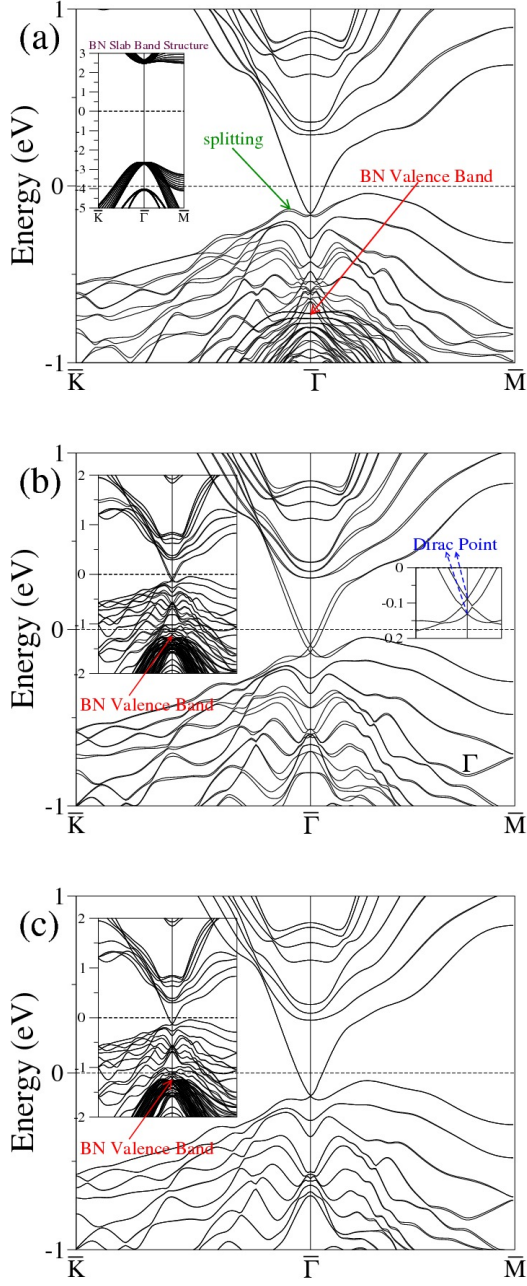


FIG. 14: Band structure of $\text{Bi}_2\text{Te}_2\text{Se}/\text{BN}$ supercell along high symmetry directions of the hexagonal BZ for *asymmetric* capping cases (a) B on the top of Te on one side and vacuum on the other side of TI film and (b) B on the top of Te atom on one side and N on the top of Te atom on the other side and for *symmetric* capping case (c) B on the top of Te on both sides of TI film. The atomic relaxation is not considered. The Dirac cone at the $\bar{\Gamma}$ -point is not disturbed in the presence of crystalline BN thin film. The fourfold degeneracy is lifted to two twofold degeneracies at the $\bar{\Gamma}$ -point in the inset of (b). The position of BN valence band maximum can be found by the band structure of BN slab without TI in the inset of (a).

twofold degeneracy on each surface band still remains due

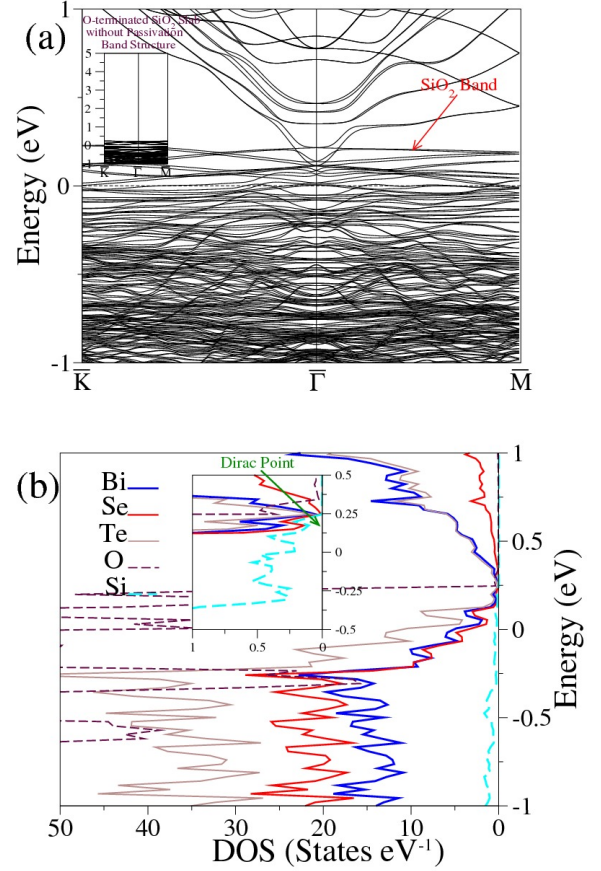


FIG. 15: (Color online) (a) Band structure of $\text{Bi}_2\text{Te}_2\text{Se}$ with oxygen-terminated quartz supercell without atomic relaxation along high symmetry directions in the hexagonal BZ suggesting that Dirac cone is affected and (b) corresponding atom-projected DOS. The Dirac point of TI is buried into quartz valence bands. Band structure of only oxygen-terminated SiO_2 slab without passivation is in the inset of (a). The Fermi level is below valence band edge formed by oxygen orbitals. The Dirac point is marked with the arrow on the inset of (b).

to Kramer's theorem which requires that the twofold degeneracy at the time-reversal invariant momenta points is protected in the absence of time-reversal symmetry breaking perturbations. On the other hands, in the *symmetric* structure of B on the top of Te on both sides, surface bands on both sides are perfectly aligned as seen in Fig. 14(c). In BN cappings of $\text{Bi}_2\text{Te}_2\text{Se}$, the bulk band gap sizes (around 0.33 eV) are a bit larger than 0.325 eV the bulk band gap of 4QLs $\text{Bi}_2\text{Te}_2\text{Se}$ without BN.

For the capping $\text{Bi}_2\text{Te}_2\text{Se}$ with the oxygen-terminated quartz without dangling bond passivation, the Dirac cone surface states are highly influenced by the oxygen dangling bond states in Fig. 15(a). From the DOS plot in Fig. 15(b), Bi, Te and Se orbitals are overlapped with oxygen orbitals near the Dirac point. The Dirac point indicated in the inset in Fig. 15(b) is within the valence bands of quartz. The DOS values for Bi, Se and Te at the Dirac point are not zero as shown in the inset because

the Dirac point is already buried under the bulk valence band maximum of $\text{Bi}_2\text{Te}_2\text{Se}^{19}$. Similarly with Bi_2Se_3 , oxygen dangling states modify Dirac cone surface states without breaking the Dirac point.

IV. SUMMARY AND CONCLUSIONS

We use a density functional based electronic structure method and atom-projected DOS to study the perturbations from dielectric cappings to the Dirac cone surface states of Bi-based binary and ternary TIs. Two crystalline dielectrics BN and quartz were considered with both *symmetric* and *asymmetric* cappings. Our study

suggests that oxygen coverage substantially affects the Dirac cone, consistent with a recent experimental study. All other surface dielectric terminations have no significant effect on the TI surface states.

Acknowledgments

The authors acknowledge financial support from the Nanoelectronics Research Initiative supported Southwest Academy of Nanoelectronics (NRI-SWAN) center. We thank Texas advanced computing center (TACC) for computational support (TG-DMR080016N).

-
- * Electronic address: jiwon.chang@utexas.edu
- ¹ X.-L. Qi and S.-C. Zhang, *Physics Today* **63**, 33 (2010).
 - ² M. Z. Hasan and C. L. Kane, *Rev. Mod. Phys.* **82**, 3045 (2010).
 - ³ B. Yan, H. -J. Zhang, C. -X. Liu, X. -L. Qi, T. Frauenheim, S. -C. Zhang, *Phys. Rev. B* **82**, 161108 (2010).
 - ⁴ D. Xiao, Y. Yao, W. Feng, J. Wen, W. Zhu, X. Q. Chen, G. M. Stocks, Z. Zhang, *Phys. Rev. Lett.* **105**, 096404 (2010).
 - ⁵ W. Feng, D. Xiao, J. Ding, Y. Yao, *Phys. Rev. Lett.* **106**, 016402 (2011).
 - ⁶ S. Chadov, X.-L. Qi, J. Kibler, G. H. Fecher, C. Felser, S.-C. Zhang, *Nature Mater.* **9**, 541 (2010).
 - ⁷ H. Lin, L.A. Wray, Y. Xia, S. Jia, R.J. Cava, A. Bansil, M.Z. Hasan, *Nature Materials* (2010).
 - ⁸ H. Zhang, C. -X. Liu, X. -L. Qi, X. Dai, Z. Fang and S.-C. Zhang, *Nature Physics* **5**, 438 (2009).
 - ⁹ A.A. Burkov, D.G. Hawthorn, *PRL* **105**, 066802 (2010).
 - ¹⁰ Y. S. Hor, P. Roushan, H. Beidenkopf, J. Seo, D. Qu, J. G. Checkelsky, L. A. Wray, D. Hsieh, Y. Xia, S.-Y. Xu, D. Qian, M. Z. Hasan, N. P. Ong, A. Yazdani, R. J. Cava, *Phys. Rev. B* **81**, 195203 (2010).
 - ¹¹ J. P. Perdew, K. Burke and M. Ernzerhof, *Phys. Rev. Lett.* **77**, 3865 (1996).
 - ¹² C. R. Dean, A. F. Young, I. Meric, C. Lee, L. Wang, S. Sorgenfrei, K. Watanabe, T. Taniguchi, P. Kim, K. L. Shepard and J. Hone, *Nat. Nanotech.* **5**, 722 (2010).
 - ¹³ J. Xue, J. S- Yamagishi, D. Bulmash, P. Jacquod, A. Deshpande, K. Watanabe, T. Taniguchi, P. J- Herrero and B. J. LeRoy, *Nat. Mater.* **10**, 282 (2010).
 - ¹⁴ D. Kong, J. J. Cha, K. Lai, H. Peng, J. G. Analytis, S. Meister, Y. Chen, H-J Zhang, I. R. Fisher, Z-X Shen, and Y. Cui, *ACS Nano* **5** (6), 4698-4703 (2011).
 - ¹⁵ T. Ozaki and H. Kino, *Phys. Rev. B* **72**, 045121 (2005).
 - ¹⁶ T. Ozaki, *Phys. Rev. B* **67**, 155108 (2003).
 - ¹⁷ C. -X. Liu, X.-L. Qi, H. J. Zhang, X. Dai, Z. Fang, and S. -C. Zhang, *Phys. Rev. B* **82**, 045122 (2010).
 - ¹⁸ Y. Zhang, K. He, C. Z. Chang, C. L. Song, L. L. Wang, X. Chen, J. F. Jia, Z. Fang, X. Dai, W. Y. Shan, S. Q. Shen, Q. Niu, X. l. Qi, S. C. Zhang, X. C. Ma and Q. K. Xue, *Nature Physics*. **6**, 584 (2010).
 - ¹⁹ J. Chang, L. F. Register, S. K. Banerjee and B. Sahu *Phys. Rev. B* **83**, 235108 (2011).
 - ²⁰ <http://cst-www.nrl.navy.mil/lattice/struk/bk.html>.
 - ²¹ K. Watanabe, T. Taniguchi, and H. Kanda, *Nat. Mater.* **3**, 404 (2004).
 - ²² <http://cst-www.nrl.navy.mil/lattice/struk/sio2a.html>.
 - ²³ E. P. O'Reilly and J. Robertson, *Phys. Rev. B* **27**, 3780 (1983).